

Supporting Information

Competitive Photooxidation of Small Colorless Organics Controlled by Oxygen Vacancies under Visible Light

Jianghui Sun^{‡ [a,b]}, Xiyang Ge^{‡ [a]}, Yixuan Gao^[a], Min Zhang^[a], Qi Zhao^[a], Guohua Hou^[a], Xiaoni Wang^[a], Yiyang Yin^[a], Jin Ouyang^[c] and Na Na^{*[a]}

[a] Key Laboratory of Radiopharmaceuticals, Ministry of Education, College of Chemistry, Beijing Normal University, Beijing 100875, China, E-mail: nana@bnu.edu.cn

[b] State Key Laboratory of Bioactive Substance and Function of Natural Medicines, Institute of Materia Medica, Chinese Academy of Medical Sciences and Peking Union Medical College, Beijing 100050, China.

[c] Department of Chemistry, College of Arts and Sciences, Beijing Normal University, Zhuhai 519087, China

[‡] These authors contributed equally.

Experimental Procedures

Chemicals

All reagents and solvents were purchased from commercial sources and were used without further purification, unless otherwise noted. All chemicals were of analytical grade.

Instruments

All spectra were recorded on an LTQ XL (Thermo Fisher Scientific, San Jose, CA, USA) instrument. NMR spectra were recorded on JEOL-400 spectrometer. UV–vis diffuse reflectance spectra (DRS) were measured on a UV 2600 spectrophotometer (Shimadzu, Japan). Photoluminescence spectroscopy measurements were performed on a FLS980 fluorescence spectrophotometer (Edinburgh Instruments, UK). Transmission electron microscopy (TEM) imaging was performed on a FEI Talos 200s transmission electron microscope. X-ray diffraction was measured by a Maxima XRD-7000 (Shimadzu, Japan) and XPS spectra were measured by a PHI-5300 ESCA spectrometer (Perkin Elmer) equipped with an Al K α excitation source. Electron Paramagnetic Resonance (EPR) spectra were obtained from a Bruker ER200-SRC-10/12 spectrometer. The photocurrent and electrochemical impedance spectra were collected on a CHI 660e electrochemical workstation. Raman spectra were recorded using a Raman spectrometer (Horiba Jobin Yvon S.A.S.) with a 532 nm laser as the excitation source.

Results and Discussion

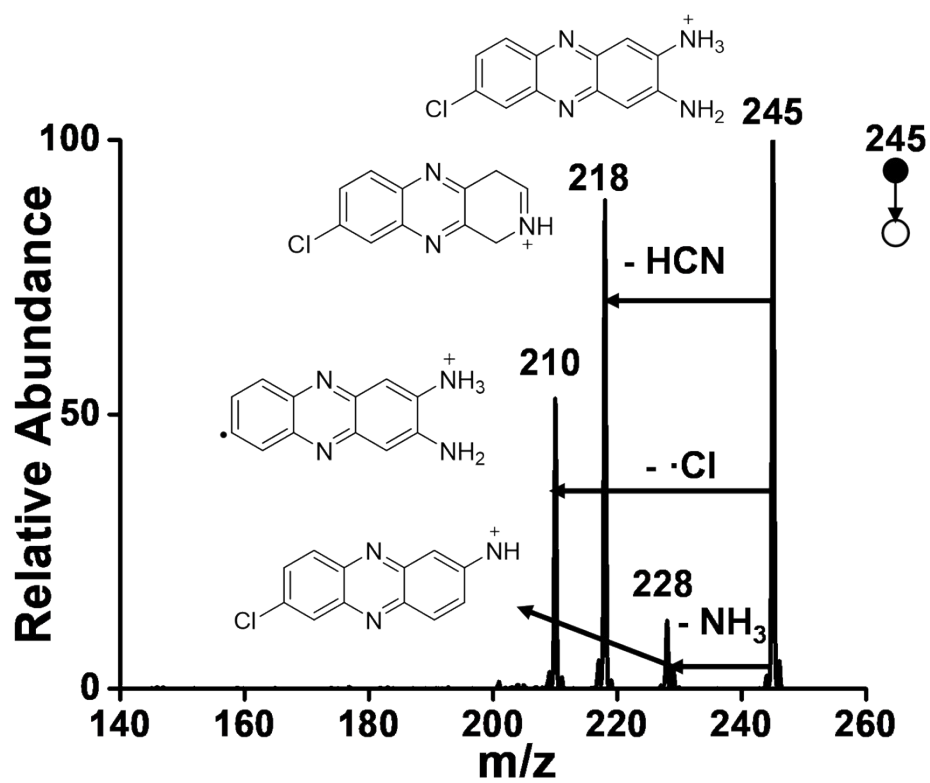


Figure S1. CID experiments to examine product ion of $[7\text{-Cl-Phz+H}]^+$ at m/z 245.

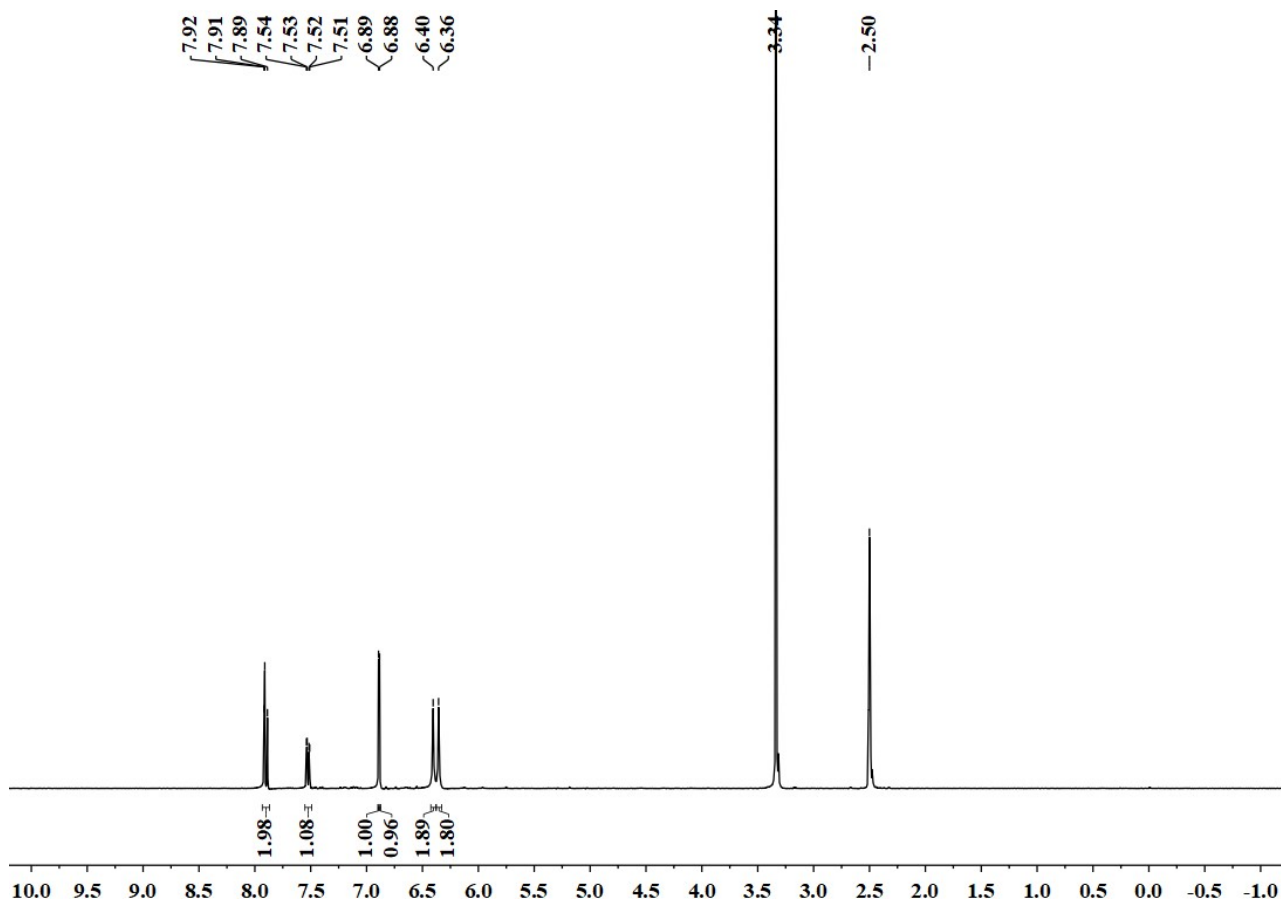


Figure S2. ^1H NMR of product 7-Cl-Phz (CD_3OD , 400 MHz).

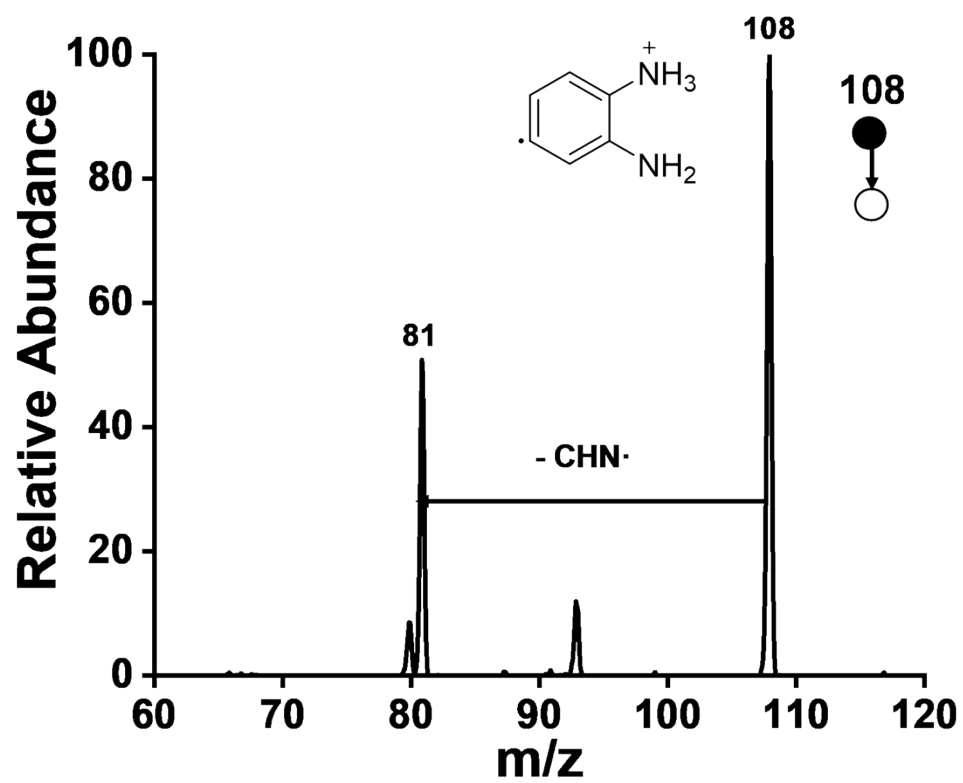


Figure S3. MS^n of dechlorination product ion at m/z 108.

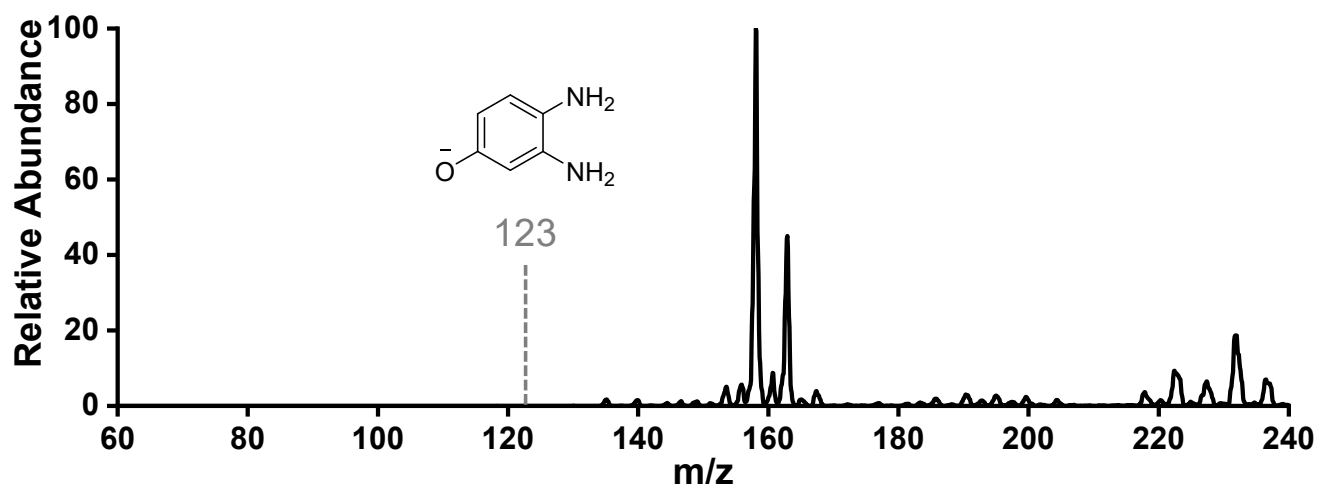


Figure S4. Mass spectra of the reaction system in negative mode.

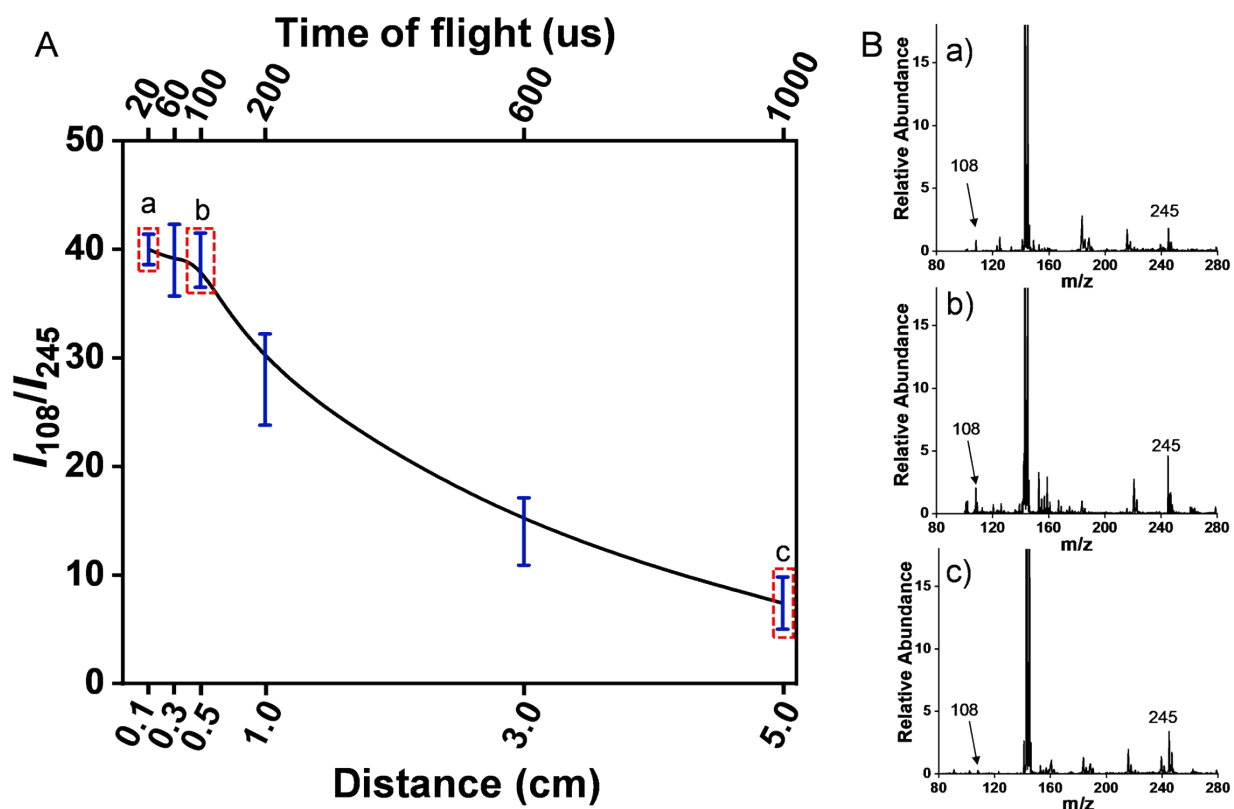


Figure S5. Evaluation on the effect of transfer distance from spray tip to MS inlet on detecting o -PD⁺. (A) Changes of the ratio of o -PD⁺ (m/z 108) to 7-Cl-Phz (m/z 245) (I_{108}/I_{245}) with increasing the distance between capillary tip and MS inlet. (B) Mass spectra obtained by MF-EESI monitoring at the transfer distance of 0.1 cm (a), 0.5 cm (b) and 5.0 cm (c). The reaction system was irradiated for 1.5 min (kinetic equilibrium of o -PD[•]) before spraying out of the capillary.

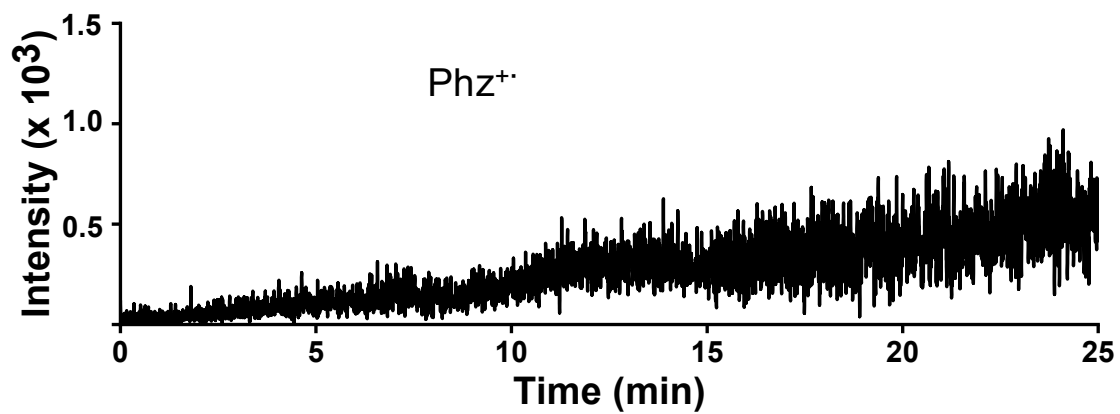


Figure S6. EIC of Phz⁺ (m/z 210) degraded from 7-Cl-Phz.

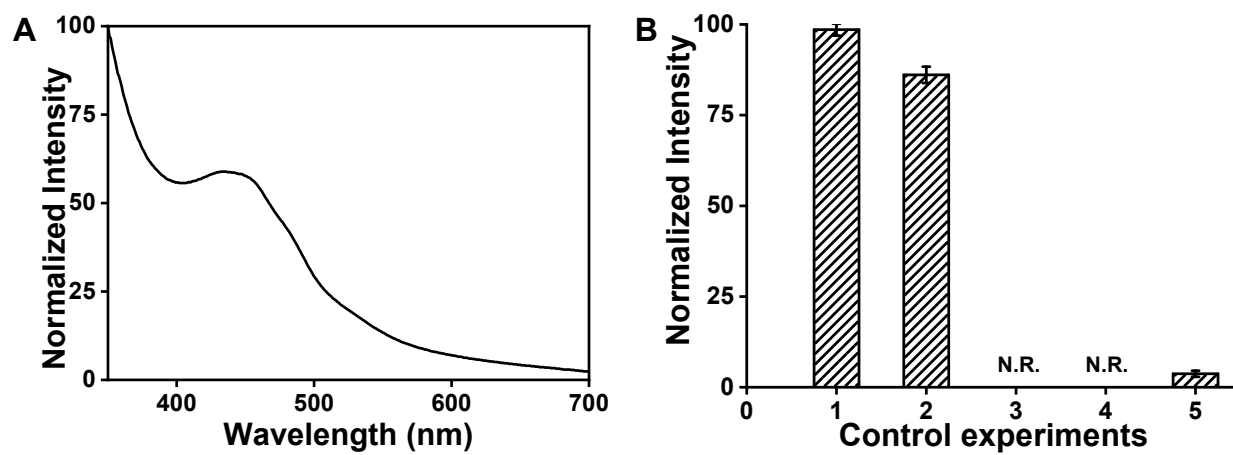


Figure S7. (A) UV-vis absorption signals of the reaction solution after irradiating for 25 min. (B) Control experiments. **1:** standard conditions; **2:** adding 0.1 mg 7-Cl-Phz; **3:** without TiO₂; **4:** without light; **5:** without O₂.

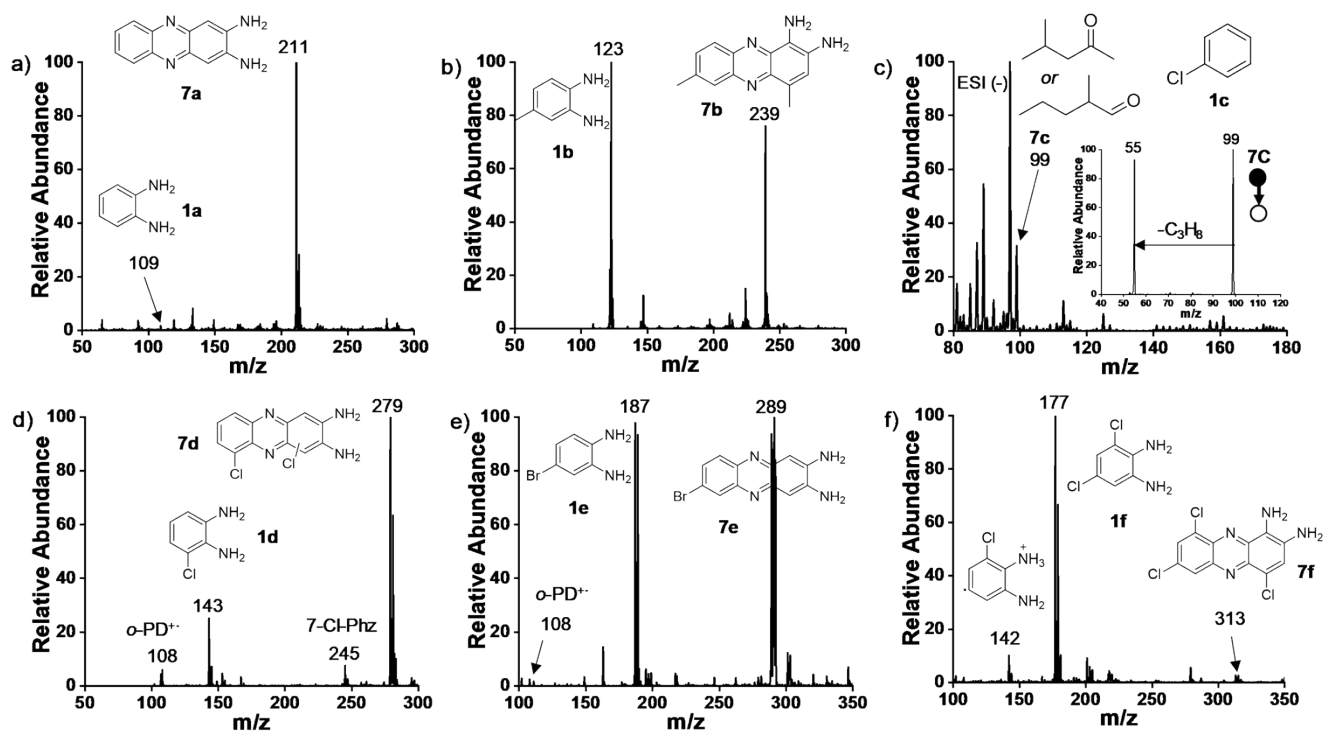


Figure S8. Substrate scope investigation for competitive photooxidations.

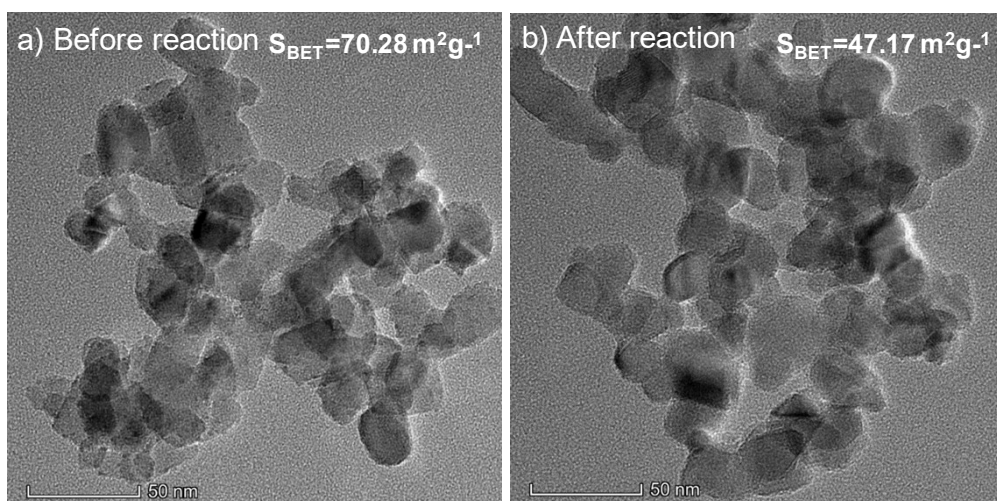


Figure S9. TEM and N_2 adsorption characterization of TiO_2 before (a) and after (b) the reaction.

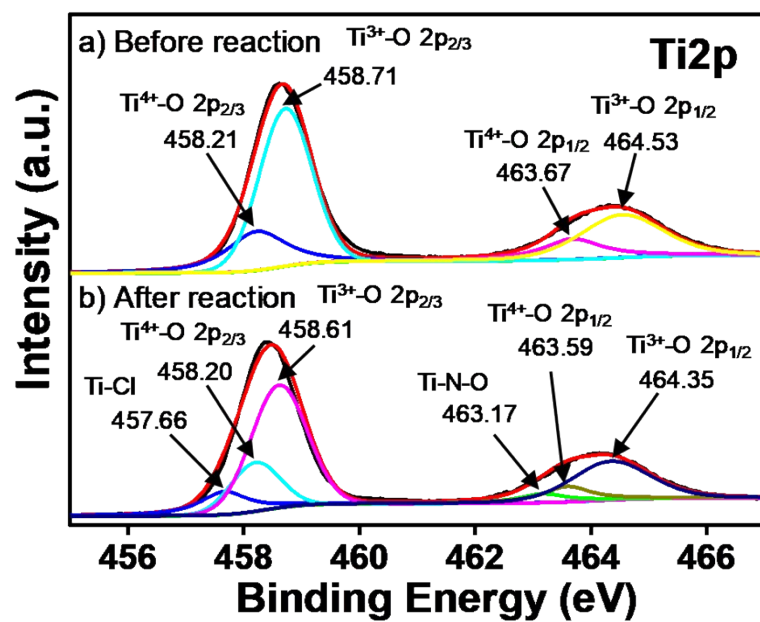


Figure S10. Core level HR-XPS spectra in Ti 2P region of TiO₂ before (a) and after (b) the reaction.

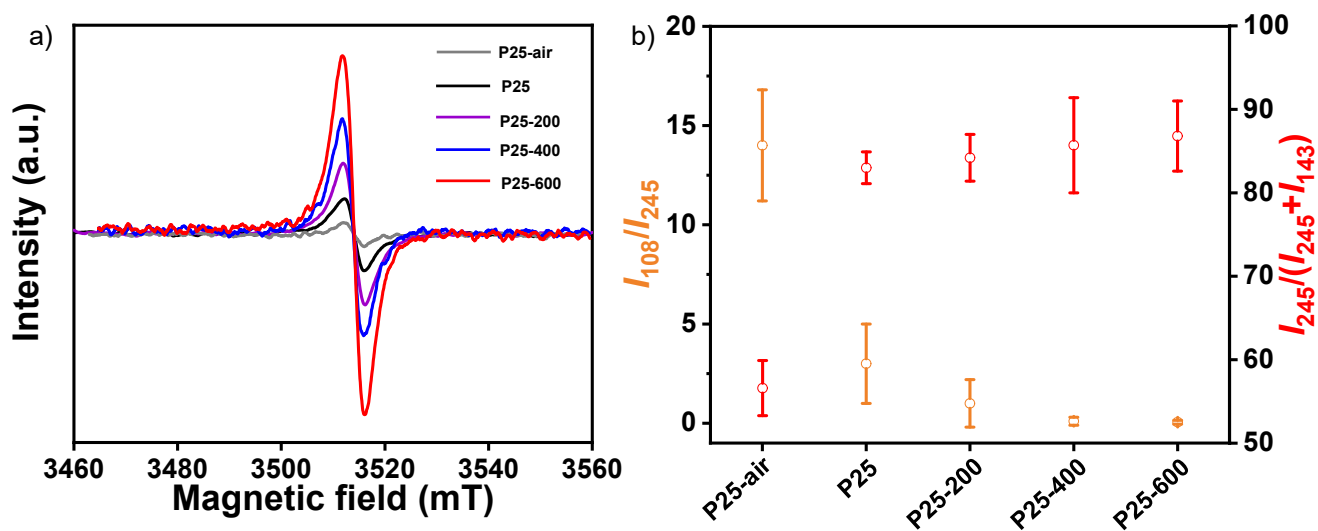


Figure S11. Evaluation of competitive photooxidation performance catalyzed by TiO₂ with varying OV levels. (a) EPR spectra of TiO₂ catalysts with different OV concentrations. (b) The corresponding yields [$I_{245}/(I_{245}+I_{143})$] and ratios of degradation product ion (m/z 108) to coupling product ion (m/z 245) (I_{108}/I_{245}).

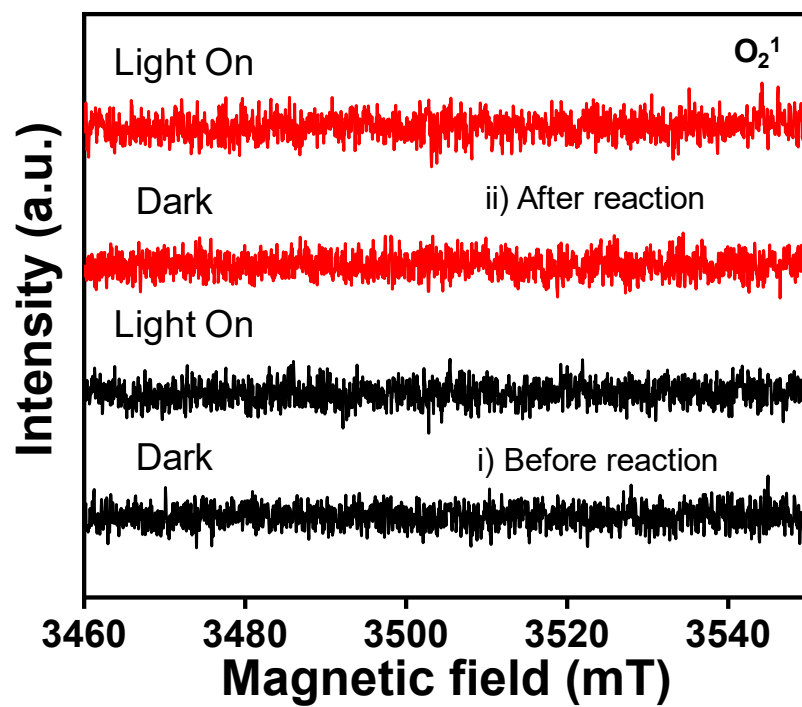


Figure S12. EPR spectra of O_2^1 in dark and under photoirradiation.

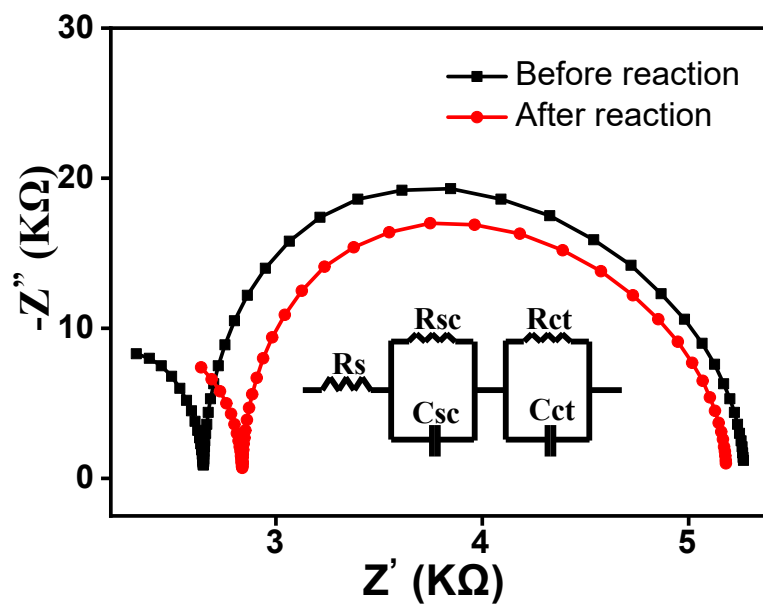


Figure S13. Nyquist plots of TiO_2 before and after the reaction.

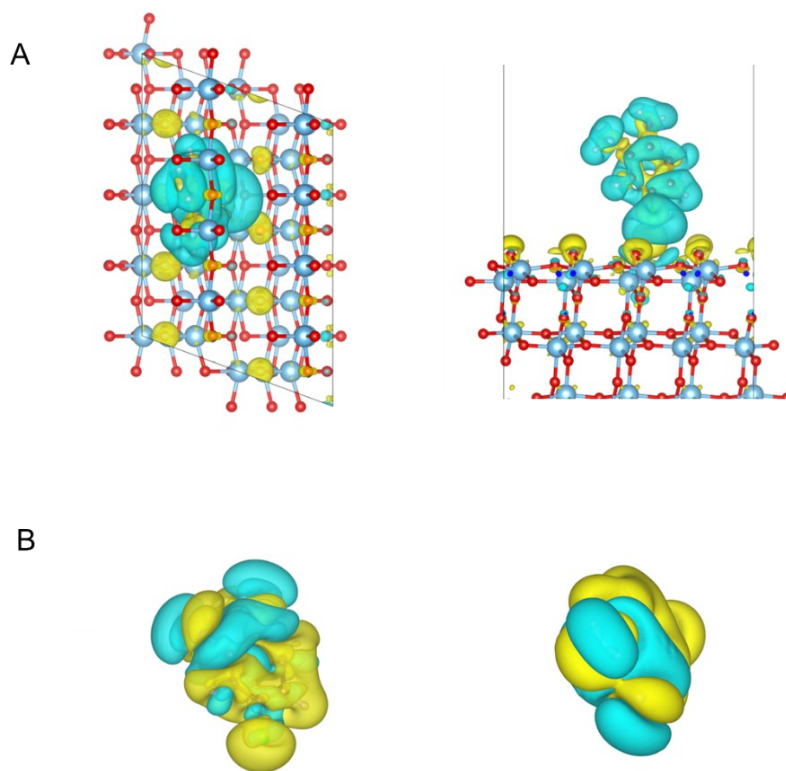


Figure S14. Top and side views of the Charge Density Difference Analysis of (A) **o*-CAN in Ti-Cl mode and (B) *o*-CAN molecular. The yellow and the cyan areas represent charge accumulation and depletion, respectively. The isosurface value is taken as $0.00022 \text{ e} \cdot \text{bohr}^{-3}$.

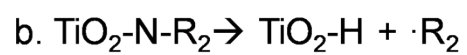
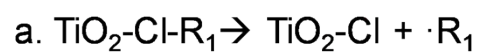
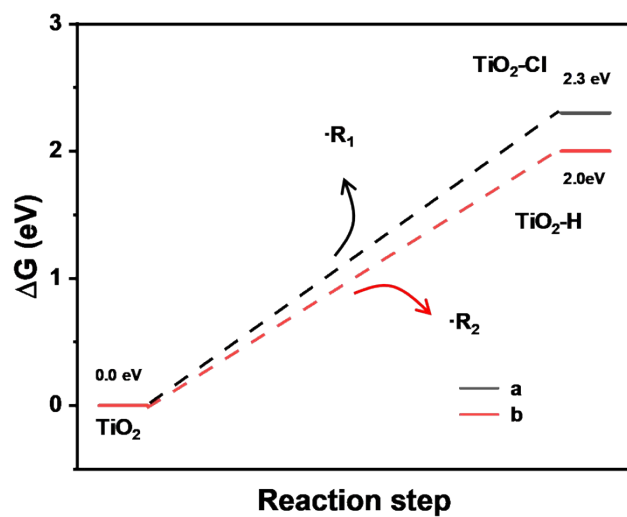


Figure S15. Free energy changes of dichlorination and dehydrogenation on TiO_2 without OVs.

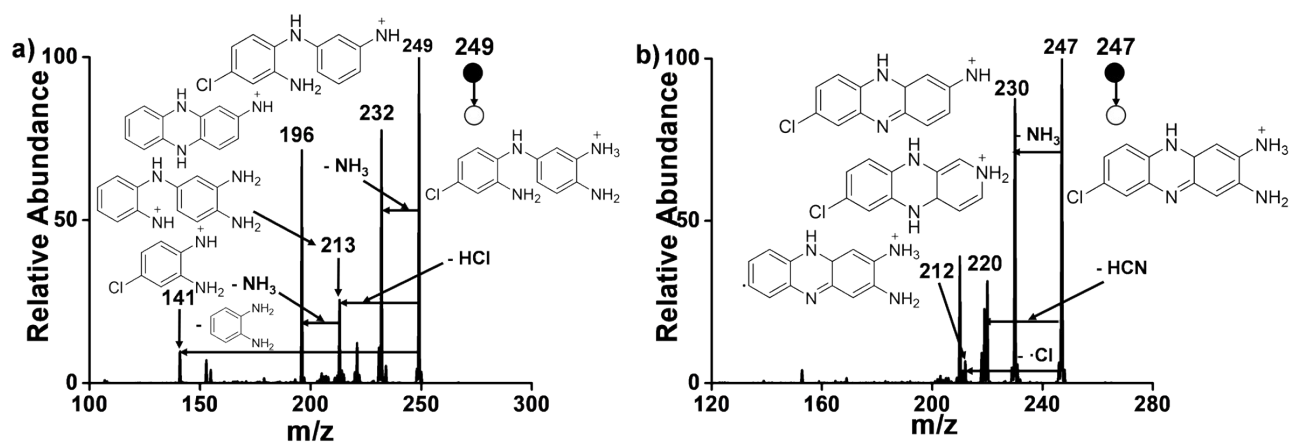


Figure S16. MSⁿ of intermediate ions at m/z 249 (a) and m/z 247 (b).

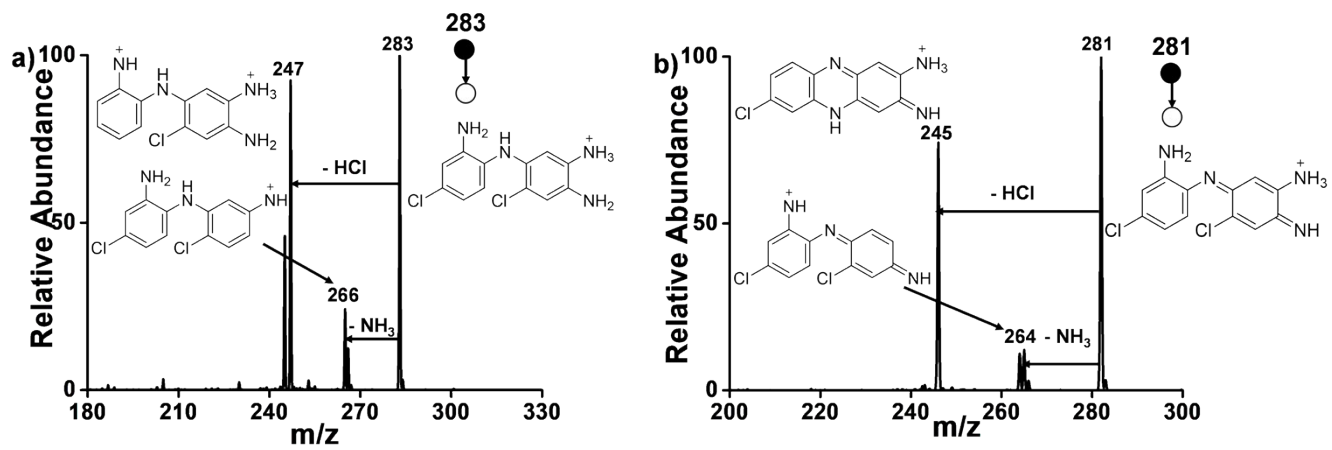


Figure S17. MSⁿ of intermediate ions at m/z 283 (a) and m/z 281 (b).

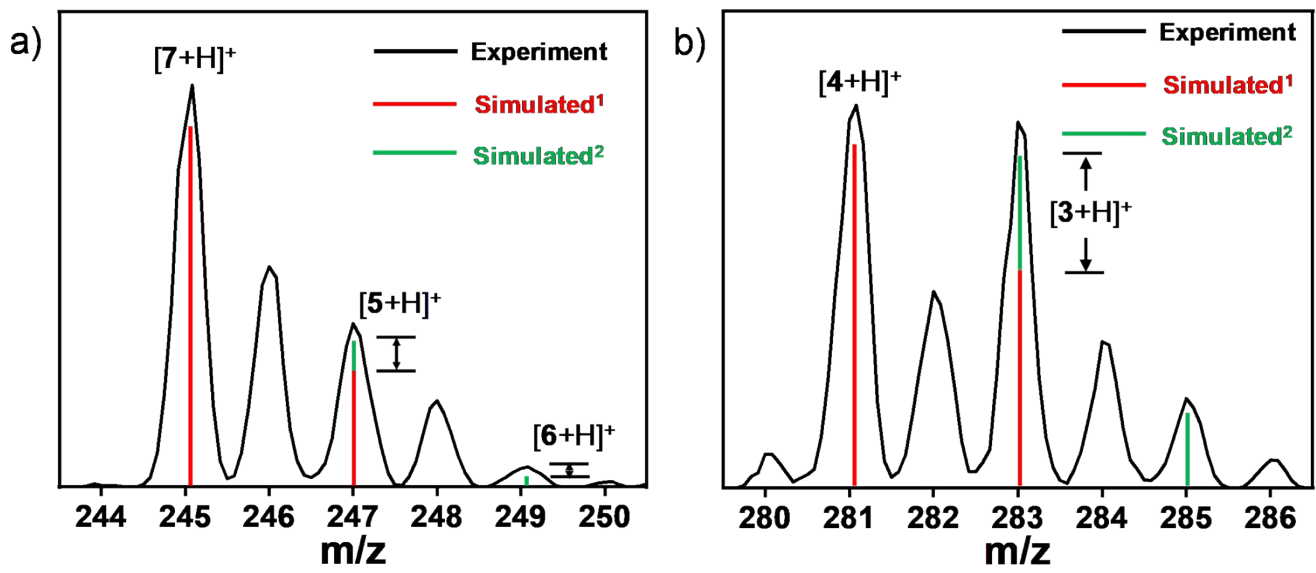


Figure S18. Observed isotopic distributions of intermediate 7, 5 and 4 for the comparison with the natural isotopic distributions.

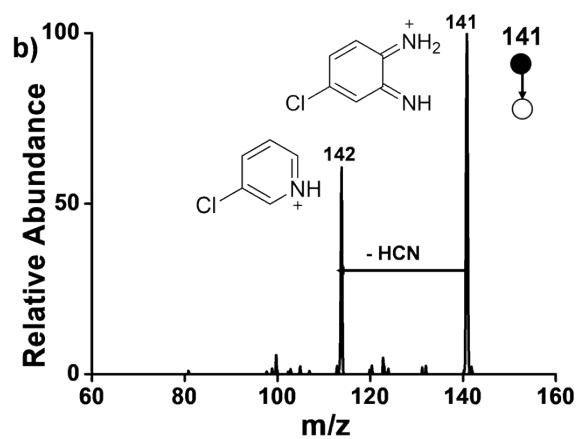
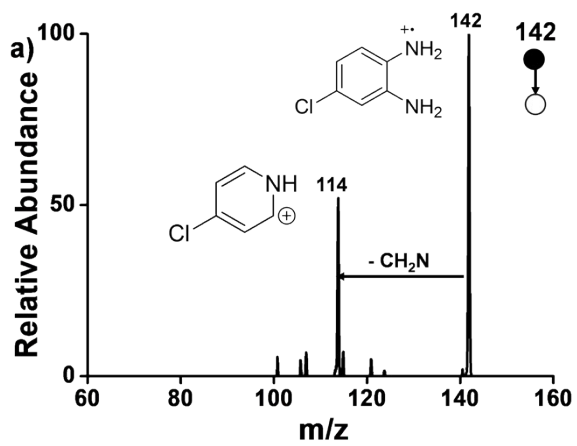


Figure S19. MSⁿ of intermediate ions at m/z 142 (a) and m/z 141 (b).